Foreground and background dust in star cluster directions

C.M. Dutra[1] **and E. Bica**[1]

Universidade Federal do Rio Grande do Sul, IF, CP 15051, Porto Alegre 91501–970, RS, Brazil

Abstract. This paper compares reddening values E(B-V) derived from the stellar content of 103 old open clusters and 147 globular clusters of the Milky Way with those derived from DIRBE/IRAS 100 μm dust emission in the same directions. Star clusters at $|b| > 20°$ show comparable reddening values between the two methods, in agreement with the fact that most of them are located beyond the disk dust layer. For very low galactic latitude lines of sight, differences occur in the sense that DIRBE/IRAS reddening values can be substantially larger, suggesting effects due to the depth distribution of the dust. The differences appear to arise from dust in the background of the clusters consistent with a dust layer where important extinction occurs up to distances from the Plane of $\approx$ 300 pc. For 3 % of the sample a significant background dust contribution might be explained by higher dust clouds. We find evidence that the Milky Way dust lane and higher dust clouds are similar to those of several edge-on spiral galaxies recently studied in detail by means of CCD imaging.

Key words: Galaxy: globular clusters: general – Galaxy: open clusters and associations: general – ISM: dust, extinction

1. Introduction

Full-sky surveys in the far infrared have been achieved by means of the IRAS and COBE satellite observations. Schlegel et al. (1998) built a reddening map from the 100 μm IRAS dust emission distribution considering temperature effects using 100/240 μm DIRBE data. The transformation to E(B-V) maps was obtained from dust columns calibrated via the (B-V)-Mg2 relation for early type galaxies. This far-infrared reddening (hereafter E(B-V)$_{FIR}$) presents a good agreement at high galactic latitudes with that derived from H I and galaxy counts by Burstein & Heiles (1978, 1982) with an offset of 0.02 mag (lower values for the latter method). Recently, Hudson (1999) analysed E(B-V)$_{FIR}$ maps using 50 globular clusters with $|b| > 10°$ and distance from the plane $|Z| > 3$ kpc, as well as 86 RR Lyrae from Burstein & Heiles (1978). These two samples provided slightly lower values on the average as compared to Schlegel et

al.'s reddening values (ΔE(B-V) = -0.008 and -0.016, respectively). The reddening comparisons above hardly exceed the limit E(B-V) $\approx$ 0.30, so that a more extended range should be explored.

Since the Galaxy is essentially transparent at 100 μm, the far-infrared reddening values should represent dust columns integrated throughout the whole Galaxy in a given direction. Star clusters probing distances as far as possible throughout the Galaxy should be useful to study the dust distribution in a given line of sight. Globular clusters and old open clusters are ideal objects for such purposes because they are in general distant enough to provide a significant probe of the galactic interstellar medium and have a suitable sky coverage. Clearly, star clusters beyond the disk dust layer are expected to have reddening values essentially comparable to those of galaxies in the same direction. On the other hand, clusters within the dust layer should have contributions from clouds in background regions. Another issue is the thickness of the Milky Way dust lane and whether some dust clouds occur at higher distances from the Plane. Recently, several edge-on spiral galaxies have been studied in detail (Howk & Savage 1999) and a comparison of their dust distribution with that of the Milky Way is worthwhile.

The aim of the present study is to compare star cluster reddening values measured from direct methods, i.e. sampling the dust effects seen in the light emitted by the cluster members, with those derived from the 100 μm dust emission. We investigate the possibility of background and foreground dust contributions in star cluster directions. In Sect. 2 we present an overview of Schlegel et al.'s (1998) reddening values predicted in different environments in the Galaxy. In Sect. 3 we gather the necessary data for globular clusters and old open clusters and describe the sample properties. In Sect. 4 we discuss the results, especially the star cluster lines of sight with evidence of background dust. Finally, the concluding remarks are given in Sect. 5.

2. Overview of dust emission reddening values E(B-V)$_{FIR}$

For a better understanding of the reddening distribution throughout the Galaxy we extracted E(B-V)$_{FIR}$ values from Schlegel et al.'s maps using the software *dust-getval* provided by them. We discuss (i) directions along the galactic plane which accumulate reddening from sources in different arms and other large
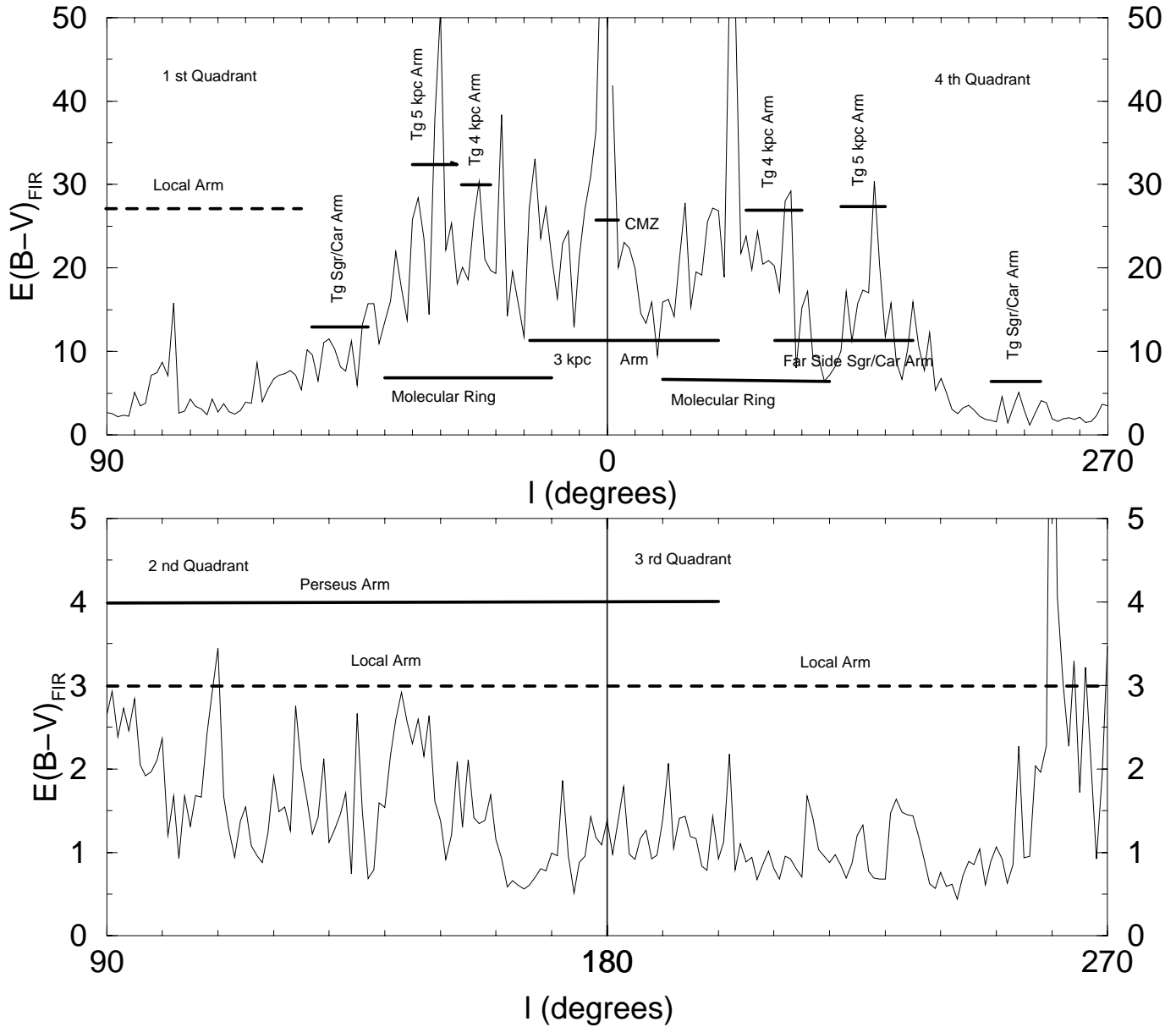
Fig. 1. Reddening distribution in the Galactic Plane derived from dust emission (Schlegel et al. 1998). The lines indicate the limits in galactic longitude of the spiral arm features and other large scale structures (see the text)

structures, and (ii) galactic latitude profiles to see the effects of relatively isolated nearby (high latitude) dust clouds.

We show in Fig. 1 the entire Galaxy longitude profile. The upper panel is in direction of the galactic centre and the lower one is in direction of the anticentre. Note the enormous reddening differences between the two panels: the lower panel has typical values of $E(B-V)_{FIR} \approx 1.5$, and the values in the upper panel are a factor ≈ 10 higher. We indicate a series of H I, CO and optical features which help interpret the reddening distribution: (i) tangent regions of the spiral arms Sagittarius-Carina, Scutum (5 kpc arm) and 4 kpc arm (Henderson 1977; Georgelin & Georgelin 1970a; Cohen et al. 1980); (ii) the extent of the 3 kpc arm (Kerr & Hindman 1970; Bania 1980); (iii) the extent of the far-side of the Sagittarius-Carina arm (Grabelsky et al.

1988); (iv) the Molecular Ring (MR) and the Central Molecular Zone (CMZ), (Combes 1991; Morris & Serabyn 1996); and finally, (v) the extent of the Local (Orion) and Perseus arms (Georgelin & Georgelin 1970b).

The relatively low reddening in the anticentre panel can be basically explained by the cumulative effect of the three external arms: Orion, Perseus and Outer arm (Digel et al. 1990). It is worth noting that $E(B-V)_{FIR}$ on the average is higher in the second quadrant than in the third quadrant, probably by the interruption of the Perseus arm. The steady increase of $E(B-V)_{FIR}$ in the first and fourth quadrants towards the direction of the Galactic center can be explained by the cumulative effect of inner arms and especially their tangent zones. Owing to the 100 μm dust emission transparency the far side arms of the
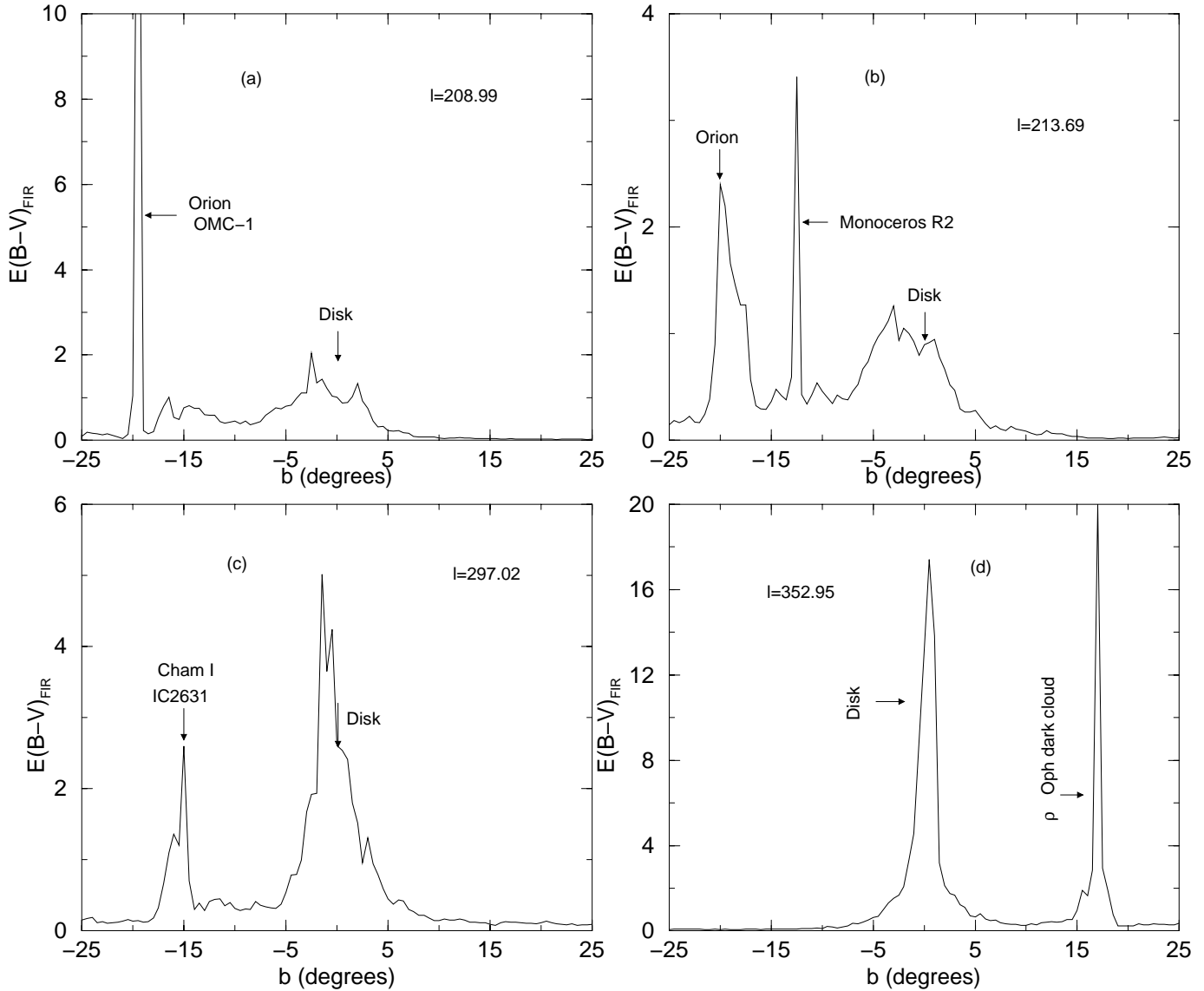
Fig. 2a–d. E(B-V)$_{FIR}$ reddening profiles in galactic latitude including relatively high dark clouds: **a** Orion Molecular Cloud 1, **b** Monoceros R2, **c** Chamaeleon I dark cloud centred at the reflection nebula IC 2631, and **d** ρ Ophiuchi dark cloud centred at the molecular cloud core IR star cluster. The longitude is indicated in each panel

Galaxy will also contribute to E(B-V)$_{FIR}$ (see the extent of far side of the Sagittarius-Carina arm in the fourth quadrant). The Molecular Ring is also a major contributor, leading to a plateau level E(B-V)$_{FIR} \approx 20$. Finally, the Central Molecular Zone is responsible for the central cusp.

Fig. 2 shows E(B-V)$_{FIR}$ profiles in the interval $-25° \leq b \leq 25°$ for selected galactic longitudes including well-known dark cloud centers. The individual clouds, especially their central parts can attain comparable (in some cases higher) E(B-V)$_{FIR}$ values to disk zones at lower latitudes. Individual dark clouds have a core-halo structure. In the ρ Oph dark cloud the core FWHM is 35' while at E(B-V)$_{FIR} = 0.5$ the halo diameter is 4°. For the Chamaeleon I complex the core FWHM is 48' (in the region of the reflection nebula IC 2631) while the halo diameter at E(B-V)$_{FIR} = 0.5$ is 2.9°. From these simple comparisons

and corresponding solid angles the zones responsible for the accumulation of reddening throughout the arms appear to be the cloud halos rather than the cores, possibly combined with diffuse galactic dust.

2.1. Comparison with reddening values from JHK photometry for nearby dark clouds

We show in Table 1 embedded infrared star clusters and T Tauri groups which are related to nearby dust complexes. They can be useful to analyse the high extinction regime and to compare Schlegel et al.'s reddening values with those measured directly from Infrared (JHK) photometry of the stellar content. We give E(B-V)$_{FIR}$ values for the central positions of these stellar aggregates and indicate to which complexes they belong. The identi-

Table 1. Dust emission reddening in selected regions

ℓ (°)	b (°)	Object	E(B-V) FIR	C
192.45	-11.31	Barnard 30 T Tau Group	1.7	1
196.82	-10.55	Barnard 35 T Tau Group	0.3	1
205.17	-14.13	NGC 2071 IR Cluster	20.5	2
205.33	-14.31	M 78(NGC 2068) IR Cluster	33.6	2
206.47	-16.32	NGC 2024 IR Cluster	44.9	2
206.85	-16.53	NGC 2023 IR Cluster	2.1	2
208.55	-19.19	OMC-3 IR Cluster	7.8	3
208.82	-19.24	OMC-2 IR Cluster	11.4	4
208.99	-19.38	OMC-1 IR Cluster	50.9	5
212.43	-18.99	L 1641 South IR Cluster	10.5	6
210.08	-19.83	HH 34/KMS 12 IR T group	2.3	6
210.09	-19.58	L 1641 North IR cluster	2.2	6
210.43	-19.73	V 380 Ori IR cluster	4.8	6
210.80	-19.50	KMS 35 IR cluster	3.1	6
210.91	-19.33	KMS 36 IR T Tau Group	4.1	6
210.97	-19.33	L 1641C IR T Tau Group	4.6	6
212.23	-19.36	CK T Tau Group	3.9	6
213.69	-12.60	Mon R2 IR Cluster	2.5	7
297.02	-14.92	IC 2631(Ced 112) T Tau Group	6.2	8
297.35	-15.75	Ced 110/111 T Tau Group	2.0	8
352.95	16.96	ρ Oph Dk Cloud IR Cluster	18.6	9

Notes to Table 1 - Column 5 referred a cloud complex: 1- Orion Head, 2- Orion: in Giant Molecular Cloud L 1630, 3- Orion Molecular Cloud 3, 4- Orion Molecular Cloud 2, 5- Orion Molecular Cloud 1, 6- Orion: in Giant Molecular Cloud L 1641, 7- Monoceros R2, 8- Chamaeleon I Dark Cloud, 9- ρ Ophiuchi Cloud

fications and locations of these objects are from: (i) Gomez & Lada (1998) for the T Tauri groups related to the dark clouds Barnard 30 and 35; (ii) Lada et al. (1991) for the infrared clusters embedded in the nebulae NGC 2071, M 78, NGC 2023 and NGC 2024 in the Orion Complex LDN 1630 Molecular Cloud; (iii) Minchin et al. (1991), Jones et al. (1994) and Reipurth et al. (1999 and references therein) respectively for the three deeply embedded clusters OMC-1, OMC-2 and OMC-3 in Orion Complex Molecular clouds; (iv) Strom et al. (1993) for the 7 objects in the Orion complex LDN 1641 Molecular Cloud; (v) Carpenter et al. (1997) for the Mon R2 IR cluster; (vi) Lawson et al. (1996) for two concentrations of T Tauri stars around the reflection nebulae IC 2631 and Cederblad 110/111 in the Chamaeleon I dark cloud; (vii) Comerón et al. (1993 and references therein) for the ρ Ophiuchi IR cluster. The larger E(B-V)$_{FIR}$ values occur for IR star clusters, while the T Tauri groups tend to be associated with lower reddening values. This must reflect the need of higher dust densities for the formation of star clusters and massive stars, conditions which occur in the cores of Giant Molecular Clouds in contrast to less massive dark clouds (e.g. Comerón et al. 1993; Carpenter et al. 1997).

For the infrared photometric reddening comparisons with E(B-V)$_{FIR}$ we adopt a total to selective extinction ratio $R = \frac{A_V}{E(B-V)} = 3.1$. When the original studies do not express their results in terms of A_V, we adopt the ratios $\frac{A_J}{A_V} = 0.276$, $\frac{A_H}{A_V} = 0.176$ and $\frac{A_K}{A_V} = 0.112$ from Schlegel et al. (1998).

JHK photometry of embedded stars in NGC 2024 (Comerón et al. 1996) indicates an average E(B-V) ≈ 14.5, lower than that given by E(B-V)$_{FIR}$ (Table 1) which might be accounted for if the sources are not the deepest embedded ones and if there still is a considerable amount of dust in the back half of the cloud. Another possibility is that hot stars heat the cloud core beyond the upper limit (21°K) available in Schlegel et al.'s temperature maps.

HK photometry of deeply embedded stars in OMC-2 (Johnson et al. 1990) provided an average $E(B - V) = 7.7$, so that the reddening through the whole cloud should be twice as much. These values are consistent with E(B-V)$_{FIR}$ = 11.4 (Table 1).

JHKL photometry of a deeply embedded source in OMC-1 (Minchin et al. 1991) indicated $A_L = 6$ and $A_K > 9$ which implied $A_V \approx 200$ or 90 depending on models with large and small dust grain respectively. The latter values convert to E(B-V) = 64.5 or 29.0 respectively, which bracket that from E(B-V)$_{FIR}$ = 50.9 (Table 1), in this case favouring the large grain model.

JHK measurements of stars in the Mon R2 IR cluster (Carpenter et al. 1997) indicated that most of the embedded stars are in the range $3.3 \leq E(B - V) \leq 4.5$ somewhat higher than E(B-V)$_{FIR}$ = 2.5.

McGregor et al. (1994) obtained JHK photometry of a star projected close to the center of the reflection nebula Ced110 in Chamaeleon I. They derived E(B-V) ≈ 2.4 or 5.6 depending on the assumed spectral type. In this direction E(B-V)$_{FIR}$ = 3.25, in reasonable agreement.

Comerón et al. (1993) estimated from JHK photometry that deeply embedded sources in the ρ Oph dark cloud core have $E(B - V) > 16$ and that field stars in the background of the cloud are possibly affected by E(B-V) ≈ 22.5. These values bracket that of E(B-V)$_{FIR}$ (Table 1) which is sensitive to reddening arising from the cloud as a whole.

Finally, we compare reddening values for the old/young components of the galactic nucleus (Catchpole et al. 1990; Krabbe et al. 1991), and for the two young star clusters projected close to the nucleus which contain WR stars (Quintuplet cluster = AFGL2004 and the Arches cluster = Object 17, respectively Glass et al. 1990; Nagata et al. 1995). The galactic center reddening is E(B-V) ≈ 9.7, that for the Quintuplet cluster E(B-V) ≈ 7.1 and that for the Arches cluster E(B-V) ≈ 10.6. The E(B-V)$_{FIR}$ values in these directions are exceedingly high (E(B-V)$_{FIR} \approx 98 - 100$). High values are expected since in this direction there is an integrated dust contribution behind the nucleus out to the disk edge. In the foreground of the nucleus we have contributions from the central molecular zone, the molecular ring and the four arms between the sun and the galactic nucleus. By symmetry arguments considering that there are three extra arms in the background outside the solar circle Schlegel et al.'s reddening values should not exceed E(B-V)$_{FIR} \approx 25$. A possible explanation is that the dust temperature in the nucleus and surroundings is significantly higher than those in Schlegel et al.'s temperature map. Indeed the possibility of non-thermal photon flux and existence of three massive young clusters may account for the dust heating.

We conclude that Schlegel et al.'s reddening values are in general consistent with values obtained from infrared photometry of embedded sources in dark clouds. Some discrepancies for infrared star clusters in the cores of molecular clouds might be explained by dust heated a few degrees above $21°$K. As pointed out by Schlegel et al. (1998) the same dust column density provides a factor of 5 in 100 μm flux when heated from $17°$K to $21°$K which are the temperature extremes considered in their study. For the Central Molecular Zone in the Galaxy E(B-V)$_{\rm FIR}$ values appear to be exceedingly high so that the dust temperature near the galactic nucleus must be higher. Indeed, assuming that E(B-V)$_{\rm FIR} \approx 25$ the dust temperature implied is $T \approx 26°$K.

2.2. Dust layer height from nearby dark clouds

In the following we calculate the distance from the galactic plane (Z) of the nearby dust complexes to estimate the dust layer height to which significant reddening is expected, at least in the solar neighbourhood.

Considering that the sun appears to be located 15 pc above the galactic plane (Cohen 1995; Hammersley et al. 1995), the corrected distance from the galactic plane Z' is

$$Z' = d_{\rm sun} \sin b + 15, \tag{1}$$

where d$_{\rm sun}$ is the object distance from the sun in pc.

Hipparcos distances of the Orion and ρ Ophiuchi complexes are respectively d$_{\rm sun} = 490$ pc and d$_{\rm sun} = 125$ pc (de Zeeuw et al. 1999), which imply distances from the plane $Z' = $ -148 pc and $Z' = 59$ pc respectively. The distance to Monoceros R2 is d$_{\rm sun}$ = 830 pc (Carpenter et al. 1997) and $Z' = $ -166 pc. Finally, for Chamaeleon I d$_{\rm sun} = 140$ pc (Lawson et al. 1996) and $Z' = $ -21 pc. Of these well-studied high latitude clouds Mon R2 and the Orion complex are intrinsically distant enough from the plane to estimate the dust layer height. The centers of the complexes imply $|Z'| \approx 150$ pc. Since dust in the Orion complex appears to absorb significantly (E(B-V)$_{\rm FIR} \approx 0.20$) to at least $b = $ -25° – see in Fig. 2 the b profiles for OMC-1 and Mon R2 (which includes Orion complex parts at higher latitudes), we adopt a dust layer height of 200 pc for the subsequent discussions.

3. Reddening values in star cluster directions

Since star clusters span a wide range of galactic latitudes and distances from the sun, both within and outside the dust layer, they are ideal targets for comparison of Schlegel et al.'s reddening values with those derived from the stellar content methods. In the present section we compile reddening values of globular clusters and intermediate age open clusters. Owing to their higher ages they probe the interstellar medium without being physically related to the dust complexes, except for the possibility of interactions.

3.1. Globular clusters

Harris (1996) compiled parameters for the 147 Milky Way globular clusters, keeping an updated version in the Web interface

http://physun.physics.mcmaster.ca/Globular.html.

In previous compilations, e.g. Webbink (1985), many globular clusters had scanty or no information. Colour-magnitude diagrams (CMD) based on CCD observations are now almost complete for these objects as a consequence of recent efforts, especially for the reddened low latitude globular clusters in crowded fields (e.g. Ortolani et al. 1995a; Barbuy et al. 1998a and references therein). Just to illustrate the progress achieved we mention Terzan 3 for which Webbink (1985) provided $E(B - V) = 0.32$ based on the cosecant law, but the CMD showed a considerably higher reddening $E(B - V) = 0.72$ (Barbuy et al. 1998b).

Table 2 lists the galactic globular clusters, as follows: (1) name of object, (2) and (3) galactic coordinates, (4) distance from the sun, (5) reddening derived from dust 100 μm emission E(B-V)$_{\rm FIR}$, (6) E(B-V) derived from the light emitted by the cluster members, and (7) βE(B-V) which is the difference between E(B-V)$_{\rm FIR}$ and E(B-V) (Sect. 4.1). The E(B-V)$_{\rm FIR}$ values were obtained from Schlegel et al.'s reddening maps using the cluster galactic coordinates. Reddening and distance values are from Harris' (1996) compilation as updated to June 22 1999, except for low latitude globular clusters which come from the CMD studies indicated in the table notes. Low latitude globular clusters have also been studied in detail via integrated spectral distribution in the near IR ($7000 < \lambda < 10000$ Å), which also is a direct estimator of the reddening affecting the stellar content (Bica et al. 1998). For the se clusters, reddening values derived spectroscopically were also considered in Table 2 (see table notes).

3.2. Old open clusters

The old open clusters (700 Myr or older), also usually referred to as Intermediate Age Clusters (IACs), are particularly suitable for studying the galactic reddening at low and moderately high galactic latitude directions because the old disk is relatively thick (Friel 1995). They are numerous for $90° < \ell < 270°$, thus complementary to the globular cluster sample which in turn probes numerous lines of sight towards the bulge. We looked for old open clusters in compilations (Janes & Phelps 1994; Friel 1995; Carraro et al. 1998), and individual clusters in the Open Cluster Database (Mermilliod 1996) as updated to November 1999 in the Web interface

http://obswww.unige.ch/webda.

We checked in the original references the CMD quality and the derived cluster parameters. In recent years the number of CCD photometric studies has been increasing steadily. They include clusters with CMD for the first time, CCD data on clusters previously observed photographically, and finally clusters newly observed in the infrared (J and K bands). Just to mention some recent studies: NGC 2204, NGC 2477, Berkeley 39 and Melotte 66 (Kassis et al. 1997), Trumpler 5 (Kaluzny 1998), Pişmiş 18, Pişmiş 19, NGC 6005 and NGC 6253 (Piatti et al. 1998a), Berkeley 17 and Berkeley 18 (Carraro et al. 1999), and ESO93-SC08 (Bica et al. 1999).

Table 2. Properties of Galactic globular clusters

Name	ℓ (°)	b (°)	d_{sun} (kpc)	E(B-V) FIR	E(B-V)	β E(B-V)
47 Tuc,NGC 104	305.90	-44.89	4.5	0.03	0.04	-0.01
NGC 288	152.28	-89.38	8.3	0.01	0.03	-0.02
NGC 362	301.53	-46.25	8.5	0.03	0.05	-0.02
NGC 1261	270.54	-52.13	16.4	0.01	0.01	0.00
Palomar 1	130.07	19.03	10.9	0.20	0.15	0.05
AM 1,E 1	258.36	-48.47	121.9	0.01	0.00	0.01
Eridanus,ESO551-SC1	218.11	-41.33	90.2	0.02	0.02	0.00
Palomar 2	170.53	-9.07	27.6	1.21	1.24	-0.03
NGC 1851	244.51	-35.04	12.1	0.04	0.02	0.02
M79,NGC 1904	227.23	-29.35	12.9	0.04	0.01	0.03
NGC 2298	245.63	-16.0	10.7	0.22	0.14	0.08
NGC 2419	180.37	25.24	84.2	0.06	0.11	-0.05
Pyxis,Weinberger 3	261.32	7.00	39.4	0.32	0.21	0.11
NGC 2808	282.19	-11.25	9.3	0.23	0.23	0.00
E 3,ESO37-SC1	292.27	-19.02	4.3	0.34	0.30	0.04
Palomar 3	240.14	41.86	92.7	0.04	0.04	0.00
NGC 3201	277.23	8.64	5.2	0.26	0.21	0.05
Palomar 4	202.31	71.80	109.2	0.02	0.01	0.01
NGC 4147	252.85	77.19	19.3	0.03	0.02	0.01
NGC 4372	300.99	-9.88	5.8	0.56	0.39	0.17
Rup 106	300.89	11.67	21.2	0.17	0.20	-0.03
M 68,NGC 4590	299.63	36.05	10.2	0.06	0.05	0.01
NGC 4833	303.61	-8.01	6.0	0.33	0.33	0.00
M 53,NGC 5024	332.96	79.76	18.3	0.03	0.02	0.01
NGC 5053	335.69	78.94	16.4	0.02	0.04	-0.02
ωCen,NGC 5139	309.10	14.97	5.3	0.14	0.12	0.02
M 3,NGC 5272	42.21	78.71	10.4	0.01	0.01	0.00
NGC 5286	311.61	10.57	11.0	0.29	0.24	0.05
AM 4	320.28	33.51	29.9	0.05	0.04	0.01
NGC 5466	42.15	73.59	17.0	0.02	0.00	0.02
NGC 5634	342.21	49.26	25.9	0.06	0.05	0.01
NGC 5694	331.06	30.36	34.7	0.10	0.09	0.01
IC 4499	307.35	-20.47	18.9	0.22	0.23	-0.01
NGC 5824	332.55	22.07	32.0	0.17	0.13	0.04
Palomar 5	0.85	45.86	23.2	0.06	0.03	0.03
NGC 5897	342.95	30.29	12.8	0.14	0.09	0.05
M 5,NGC 5904	3.86	46.80	7.5	0.04	0.03	0.01
NGC 5927	326.60	4.86	7.6	0.51	0.45	0.06
NGC 5946,IC 4550	327.58	4.19	12.8	0.71	0.54	0.17
BH 176,ESO224-SC8	328.41	4.34	13.4[12]	0.59	0.69	-0.10
NGC 5986	337.02	13.27	10.5	0.34	0.27	0.07
Lyngå 7,BH 184	328.77	-2.79	6.7[11]	1.06	0.72[11]	0.34
Palomar 14,AvdB	28.75	42.18	73.9	0.03	0.04	-0.01
M 80,NGC 6093	352.67	19.46	10.0	0.21	0.18	0.03
M 4,NGC 6121	350.97	15.97	2.2	0.50	0.36	0.14
NGC 6101	317.75	-15.82	15.3	0.10	0.05	0.05
NGC 6144	351.93	15.70	10.3	0.71	0.32	0.39
NGC 6139	342.37	6.94	10.1	0.90	0.75	0.15
Terzan 3	345.08	9.19	6.5	0.76	0.72	0.04
M 107,NGC 6171	3.37	23.01	6.4	0.45	0.33	0.12
ESO452-SC11,C1636-283	351.91	12.10	7.8	0.52	0.49	0.03
M 13,NGC 6205	59.01	40.91	7.7	0.02	0.02	0.00

Notes to Table 2:
[1] in Sagittarius Dwarf (Ibata et al. 1994; Da Costa & Armandroff 1995); [2] Barbuy et al. (1998a); [3] Bica et al. (1998); [4] Ortolani et al. (1999a); [5] Barbuy et al. (1998b); [6] Ortolani et al. (1999b); [7] Barbuy et al. (1999); [8] Ortolani et al. (1999c); [9] Kaisler et al. (1997); [10] Rosino et al. (1997); [11] Ortolani et al. (1993); [12] Ortolani et al. (1995b); [13] Bica et al. (1995); [14] Ortolani et al. (1998).

Table 2. (continued)

Name	ℓ (°)	b (°)	d_{sun} (kpc)	E(B-V) FIR	E(B-V)	β E(B-V)
NGC 6229	73.64	40.31	30.7	0.02	0.01	0.01
M 12,NGC 6218	15.72	26.31	4.9	0.17	0.19	-0.02
NGC 6235	358.92	13.52	10.0	0.42	0.36	0.06
M 10,NGC 6254	15.14	23.08	4.4	0.29	0.28	0.01
NGC 6256,BH 208	347.79	3.31	6.4	1.72	1.03	0.69
Palomar 15	18.87	24.30	44.6	0.40	0.40	0.00
M 62,NGC 6266	353.58	7.32	6.9	0.46	0.47	-0.01
M 19,NGC 6273	356.87	9.38	8.7	0.31	0.37	-0.06
NGC 6284	358.35	9.94	14.7	0.31	0.28	0.03
NGC 6287	0.13	11.02	8.5	0.81	0.60	0.21
NGC 6293	357.62	7.83	8.8	0.62	0.41	0.22
NGC 6304	355.83	5.38	6.1	0.52	0.52	0.00
NGC 6316	357.18	5.76	11.0	0.73	0.51	0.22
M 92,NGC 6341	68.34	34.86	8.2	0.02	0.02	0.00
NGC 6325	0.97	8.00	9.6	0.95	0.89	0.06
M 9,NGC 6333	5.54	10.70	8.2	0.43	0.38	0.05
NGC 6342	4.90	9.73	8.6	0.52	0.46	0.06
NGC 6356	6.72	10.22	15.2	0.31	0.28	0.03
NGC 6355	359.58	5.43	7.2	1.21	0.75	0.46
NGC 6352	341.42	-7.17	5.7	0.35	0.21	0.14
IC 1257	16.53	15.14	25.0	0.80	0.73	0.07
Terzan 2,HP 3	356.32	2.30	6.6	2.38	1.46	0.92
NGC 6366	18.41	16.04	3.6	0.75	0.71	0.04
Terzan 4,HP 4	356.02	1.31	7.3	6.34	2.26	4.08
HP 1,BH 229	357.42	2.12	6.4	2.24	1.15	1.09
NGC 6362	325.55	-17.57	8.1	0.07	0.08	-0.01
Liller 1	354.84	-0.16	7.4[2]	11.57	2.95[2,3]	8.92
NGC 6380, Ton 1	350.18	-3.42	9.8[14]	1.54	1.11[3,14]	0.43
Terzan 1, HP 2	357.57	1.00	5.2[4]	7.05	2.38[4]	4.67
Tonantzintla 2,Piş 26	350.80	-3.42	6.4[13]	1.65	1.23[3,13]	0.42
NGC 6388	345.56	-6.74	11.5	0.41	0.40	0.01
M 14, NGC 6402	21.32	14.81	8.9	0.48	0.60	-0.12
NGC 6401	3.45	3.98	12.0[7]	0.96	0.53[7]	0.43
NGC 6397	338.17	-11.96	2.3	0.19	0.18	0.01
Palomar 6	2.09	1.78	6.4[2]	1.76	1.31[2,3]	0.45
NGC 6426	28.09	16.23	20.4	0.35	0.36	-0.01
Djorgovski 1	356.67	-2.48	5.6[2]	2.13	1.68[2,3]	0.45
Terzan 5,Terzan 11	3.81	1.67	3.6	4.27	2.50	1.77
NGC 6440	7.73	3.80	8.4	1.14	1.07	0.07
NGC 6441	353.53	-5.01	11.2	0.61	0.44	0.17
Terzan 6,HP 5	358.57	-2.16	5.4[2]	2.67	2.13[2,3]	0.54
NGC 6453	355.72	-3.87	11.2	0.67	0.61	0.06
UKS 1	5.12	0.76	7.4[2]	6.81	3.10[2,3]	3.71
NGC 6496	348.02	-10.01	11.5	0.23	0.15	0.08
Terzan 9	3.60	-1.99	4.9[6]	2.75	1.78[3,6]	0.97
ESO456-SC38, Djorg 2	2.76	-2.51	5.5[2]	1.19	0.72[2,3]	0.47
NGC 6517	19.23	6.76	10.8	1.21	1.08	0.13
Terzan 10	4.42	-1.86	4.8[2]	5.13	2.41[2]	2.72
NGC 6522	1.02	-3.93	6.1[2]	0.57	0.55[2]	0.02
NGC 6535	27.18	10.44	6.7	0.41	0.34	0.07
NGC 6528	1.14	-4.17	7.8[2]	0.75	0.52[2]	0.23
NGC 6539	20.80	6.78	8.4	1.09	0.97	0.12
NGC 6540, Djorg 3	3.29	-3.31	3.0[2]	0.64	0.60[2]	0.04
NGC 6544	5.84	-2.20	2.6	1.71	0.73	0.98
NGC 6541	349.29	-11.18	7.0	0.16	0.14	0.02
NGC 6553	5.25	-3.02	5.1[2]	1.36	0.70[2]	0.66

Table 2. (continued)

Name	ℓ (°)	b (°)	d_{sun} (kpc)	E(B-V) FIR	E(B-V)	β E(B-V)
NGC 6558	0.20	-6.03	7.4	0.46	0.44	0.02
IC 1276, Palomar 7	21.83	5.67	4.0[5]	1.40	1.16[5]	0.24
Terzan 12	8.36	-2.10	3.4[14]	2.85	1.93[3,14]	0.92
NGC 6569	0.48	-6.68	8.7	0.42	0.56	-0.14
NGC 6584	342.14	-16.41	13.4	0.11	0.10	0.01
NGC 6624	2.79	-7.91	8.0	0.26	0.28	-0.02
M 28, NGC 6626	7.80	-5.58	5.7	0.48	0.43	0.05
NGC 6638	7.90	-7.15	8.4	0.41	0.40	0.01
M 69, NGC 6637	1.72	-10.27	8.6	0.17	0.16	0.01
NGC 6642	9.81	-6.44	7.7	0.38	0.41	-0.03
NGC 6652	1.53	-11.38	9.6	0.11	0.09	0.02
M 22, NGC 6656	9.89	-7.55	3.2	0.33	0.34	-0.01
Palomar 8	14.10	-6.80	12.9	0.41	0.32	0.09
M 70, NGC 6681	2.85	-12.51	9.0	0.11	0.07	0.04
NGC 6712	25.35	-4.32	6.9	0.39	0.45	-0.06
M 54, NGC 6715[1]	5.61	-14.09	27.2	0.15	0.14	0.01
NGC 6717, Palomar 9	12.88	-10.90	7.1[8]	0.25	0.22[3,8]	0.03
NGC 6723	0.07	-17.30	8.8	0.16	0.05	0.11
NGC 6749, Be 42	36.20	-2.20	7.3[10,9]	1.77	1.45[10,9]	0.32
NGC 6752	336.50	-25.63	4.0	0.06	0.04	0.02
NGC 6760	36.11	-3.92	7.4	0.65	0.77	-0.12
M 56, NGC 6779	62.66	8.34	10.1	0.25	0.20	0.05
Terzan 7[1]	3.39	-20.07	23.2	0.09	0.07	0.02
Palomar 10	52.44	2.72	5.9[9]	2.05	1.58[3,9]	0.47
Arp 2[1]	8.55	-20.78	28.6	0.11	0.10	0.01
M 55, NGC 6809	8.80	-23.27	5.4	0.14	0.07	0.07
Terzan 8[1]	5.76	-24.56	26.0	0.15	0.12	0.03
Palomar 11	31.81	-15.58	12.9	0.23	0.34	-0.11
M 71, NGC 6838	56.74	-4.56	3.9	0.33	0.25	0.08
M 75, NGC 6864	20.30	-25.75	18.8	0.15	0.16	-0.01
NGC 6934	52.10	-18.89	17.4	0.11	0.09	0.02
M 72, NGC 6981	35.16	-32.68	17.0	0.06	0.05	0.01
NGC 7006	63.77	-19.41	41.5	0.08	0.05	0.03
M 15, NGC 7078	65.01	-27.31	10.3	0.11	0.10	0.01
M 2, NGC 7089	53.38	-35.78	11.5	0.04	0.06	-0.02
M 30, NGC 7099	27.18	-46.83	8.0	0.05	0.03	0.02
Palomar 12	30.51	-47.68	19.1	0.04	0.02	0.02
Palomar 13	87.10	-42.70	26.9	0.11	0.05	0.06
NGC 7492	53.39	-63.48	25.8	0.04	0.00	0.04

Janes & Phelps' (1994) compilation included 72 IACs while the present sample has 103 entries. The Hyades were not included due to the proximity and large angular size. Table 3 lists the galactic old open clusters, as follows: (1) name of object, (2) and (3) galactic coordinates, (4) distance from the sun, (5) age, (6) E(B-V)$_{FIR}$, (7) E(B-V), and (8) βE(B-V).

Fig. 3 shows the sample properties. The histogram gives the distribution of old open clusters as a function of the distance from the sun. It shows that the sample is probing the interstellar medium quite far, mostly in the range 1-5 kpc and in some cases as far as 10-14 kpc. The age histogram shows a steady decrease for higher ages probably related to the dissolution rate of IACs. There occurs a peak at t $\approx$ 5 Gyr which was also present in previous compilations, and the present increased sample supports its significance. A possible interpretation for this peak would be a burst of star formation in the old disk.

4. Discussion

The angular distribution in galactic coordinates of globular and old open clusters for $|b| < 20°$ is shown in Fig. 4, centred on the galactic nucleus direction. The two samples are complementary, globular clusters probe mostly the galactic central regions while the old open clusters probe mostly the anticentre regions. The most frequent values for $|b| < 10°$ are intermediate ones ($0.2 \leq E(B-V) \leq 1.0$). For higher latitudes smaller values dominate.

Reddening values for globular clusters in bulge regions often exceed E(B-V) = 1. Terzan 1, 4, 5, 6 and 10 exceed E(B-V)

Table 3. Properties of galactic old open clusters

Name	ℓ (°)	b (°)	d_{sun} (kpc)	t (Myr)	E(B-V) FIR	E(B-V)	β E(B-V)
Be 81	34.66	-1.95	3.00	1000	2.92	1.00	1.92
IC 4756,Mel-210	36.37	5.25	0.44	750	0.76	0.20	0.56
NGC 6802,Cr 400	55.32	0.94	0.93	1750	4.32	0.83	3.49
NGC 6940,Mel-232	69.90	-7.16	0.93	750	0.48	0.24	0.24
NGC 6791,Be 46	70.01	10.95	4.24	9000	0.15	0.15	0.00
NGC 6819,Mel-223	73.97	8.47	1.86	2550	0.20	0.24	-0.04
IC1311,Tr36	77.69	4.27	4.38	1200	0.65	0.45	0.20
NGC 6811,Mel-222	79.44	11.95	1.29	650	0.14	0.13	0.01
NGC 6866,Mel-229	79.54	6.86	1.49	650	0.77	0.12	0.65
Be 54	83.12	-4.14	3.80	5600	1.19	0.84	0.35
NGC 7044,Cr 433	85.86	-4.13	3.35	1770	1.03	0.67	0.36
IC 1369,Cr 432	89.56	-0.40	0.99	1450	2.69	0.60	2.09
NGC 6939,Mel-231	95.86	12.31	1.20	1800	0.39	0.50	-0.11
NGC 7226,Cr 446	101.42	-0.59	2.56	600	1.03	0.47	0.56
Ki9	101.43	-1.82	4.56	4400	0.61	0.72	-0.11
NGC 7142,Cr 442	105.42	9.45	1.95	5100	0.50	0.40	0.10
Ki 19,Basel 2	110.57	0.14	1.39	1850	2.25	0.48	1.77
NGC 7789,Mel-245	115.48	-5.35	1.84	1520	0.41	0.25	0.16
Be 99	115.95	10.11	4.90	3150	0.48	0.30	0.18
Ki 11	117.15	6.47	2.13	5800	0.97	1.00	-0.03
NGC 7762,Mel-244	117.18	5.84	0.77	1750	1.19	0.81	0.38
Be 2	119.70	-2.31	5.25	800	0.93	0.80	0.13
NGC 188,Mel-2	122.77	22.47	1.60	4900	0.09	0.09	0.00
Ki 2	122.88	-4.68	6.00	5800	0.44	0.31	0.13
Cr463	127.36	9.56	0.35	700	0.73	0.24	0.49
IC 166,Tom 3	130.07	-0.19	3.08	1200	1.15	0.80	0.35
Be 64	131.91	4.59	3.88	1000	1.07	1.04	0.03
NGC 752,Mel-12	137.17	-23.35	0.37	1700	0.05	0.04	0.01
Be 66	139.41	0.20	5.00	4700	1.43	1.25	0.18
Ki 5	143.74	-4.26	2.19	850	0.95	0.78	0.17
NGC 1245,Mel-18	146.63	-8.92	2.80	1080	0.31	0.29	0.02
NGC 1193,Cr 35	146.80	-12.17	4.01	4950	0.24	0.12	0.12
Ki 7	149.77	-1.02	2.20	690	1.81	1.25	0.56
NGC 1496,Cr 44	149.86	0.14	1.23	630	1.42	0.45	0.97
NGC 1798,Be16	160.77	4.83	3.82	1450	0.60	0.51	0.09
Ki 22,Be 18	163.62	5.01	4.67	4600	0.61	0.47	0.14
NGC 2192,Mel-42	173.41	10.63	3.47	1100	0.18	0.20	-0.02
Be 69	174.43	-1.79	2.86	890	0.84	0.65	0.19
Be 17	175.63	-3.66	2.53	9000	0.76	0.64	0.12
Ki 8	176.39	3.11	3.35	800	0.84	0.68	0.16
Be 19	176.90	-3.59	4.83	3000	0.53	0.40	0.13
NGC 1817,Cr 60	186.13	-13.12	1.97	950	0.33	0.29	0.04
NGC 2158,Mel-40	186.64	1.78	4.09	2200	0.75	0.45	0.30
Be 21	186.84	-2.51	5.40	2700	0.84	0.69	0.15
NGC 2266,Mel-50	187.78	10.27	3.38	800	0.11	0.10	0.01
NGC 2194,Mel-43	197.26	-2.33	2.65	1000	0.82	0.42	0.40
Be 29	197.97	8.02	10.50	4800	0.10	0.21	-0.11
NGC 2141,Cr 79	198.07	-5.78	4.25	2950	0.42	0.33	0.09
NGC 2420,Mel-69	198.11	19.65	2.37	2300	0.04	0.03	0.01
Be 22	199.80	-8.04	5.05	3300	0.65	0.63	0.02
Tr 5,Cr 105	202.86	1.06	2.60	4900	0.95	0.61	0.34
NGC 2355,Mel-63	203.36	11.80	2.20	800	0.14	0.12	0.02
Be 20	203.50	-17.28	8.27	4600	0.21	0.13	0.08
NGC 2236,Cr 94	204.37	-1.68	3.21	930	0.96	0.36	0.60
NGC 2395,Cr 144	204.62	13.95	0.61	1450	0.10	0.07	0.03
Biur 7,Be 31	206.25	5.12	3.74	3700	0.14	0.24	-0.10

Table 3. (continued)

Name	ℓ (°)	b (°)	d_{sun} (kpc)	t (Myr)	E(B-V) FIR	E(B-V)	β E(B-V)
Praesepe,M 44	205.53	32.52	0.17	800	0.03	0.01	0.02
NGC 2112,Cr 76	205.90	-12.59	0.80	5000	1.06	0.50	0.56
Biur 8,Be 32	207.93	4.37	3.09	4500	0.26	0.16	0.10
Cr 110	209.64	-1.97	1.95	1400	1.12	0.50	0.62
Biur 9,Be 30	210.78	2.86	2.34	900	0.63	0.61	0.02
NGC 2324,Mel-59	213.39	3.22	3.70	850	0.29	0.13	0.16
NGC 2286,Cr 117	215.31	-2.29	2.19	1600	1.26	0.03	1.23
M 67,NGC 2682	215.66	31.94	0.82	5300	0.03	0.06	-0.03
Be 39	223.46	10.08	4.40	7400	0.12	0.12	0.00
NGC 2204,Mel-44	226.01	-16.09	4.27	2150	0.10	0.09	0.01
Haf 8	227.53	1.35	1.18	1430	0.66	0.03	0.63
Haf 6	227.85	0.24	3.23	950	0.76	0.43	0.33
Mel-71,Cr 155	228.95	4.51	2.69	950	0.26	0.06	0.20
NGC 2360,Mel-64	229.79	-1.40	1.30	1250	0.82	0.08	0.74
NGC 2423,Mel-70	230.47	3.54	0.70	1200	0.32	0.12	0.20
NGC 2506,Mel-80	230.60	9.96	3.01	2250	0.08	0.09	-0.01
Tom 1,Haf 1	232.33	-7.31	3.00	1000	0.50	0.40	0.10
Tom 2,Haf 2	232.83	-6.88	9.60	2100	0.39	0.25	0.14
NGC 2539,Mel-83	233.71	11.10	1.48	600	0.07	0.08	-0.01
NGC 2243,Mel-46	239.48	-18.01	3.75	6000	0.07	0.05	0.02
NGC 2527,Cr 174	246.08	1.85	0.61	850	0.47	0.08	0.39
NGC 2533,Cr 175	247.80	1.30	1.55	1900	0.68	0.01	0.67
AM 2,ESO368SC7	248.12	-5.87	8.35	8300	0.73	0.56	0.17
NGC 2627,Mel-87	251.58	6.65	1.91	2800	0.15	0.15	0.00
NGC 2477,Mel-78	253.56	-5.83	1.12	900	0.65	0.29	0.36
Piş 3	257.86	0.49	1.35	2550	1.56	1.35	0.21
Piş 2	258.85	-3.33	2.84	1700	2.27	1.48	0.79
Mel-66,Cr 147	259.56	-14.24	2.88	5900	0.22	0.17	0.05
NGC 2818A,Mel-96	262.00	8.60	3.93	1050	0.19	0.18	0.01
NGC 2660,Mel-92	265.93	-3.00	2.89	1100	1.11	0.37	0.74
NGC 1901,Bok 1	279.04	-33.64	0.42	832	0.33	0.06	0.27
NGC 3680,Mel-106	286.76	16.93	0.90	2200	0.09	0.06	0.03
ESO92SC18	287.12	-6.65	7.90	5300	0.29	0.26	0.03
NGC 3496,Cr 237	289.51	-0.40	1.12	850	2.40	0.50	1.90
ESO93SC8	293.50	-4.04	13.70	4500	0.91	0.64	0.27
NGC 3960,Mel-108	294.36	6.18	1.68	800	0.44	0.29	0.15
Harv 6,Cr 261	301.68	-5.53	2.38	8500	0.45	0.30	0.15
AL 1,ESO96SC4	305.36	-3.16	7.57	800	0.94	0.72	0.22
IC 4291,Piş 18	308.24	0.32	2.24	1200	5.79	0.50	5.29
Piş 19	314.70	-0.30	2.40	1000	12.52	1.45	11.07
NGC 5823,Mel-131	321.12	2.45	0.71	1650	2.04	0.11	1.93
NGC 5822,Mel-130	321.57	3.59	0.83	850	0.98	0.17	0.81
NGC 6005,Mel-138	325.78	-2.98	2.69	1200	0.84	0.45	0.39
NGC 6208,Cr 313	333.75	-5.76	1.25	2050	0.33	0.15	0.18
NGC 6134,Mel-146	334.91	-0.19	0.88	1150	25.66	0.39	25.27
NGC 6253,Mel-156	335.45	-6.25	1.51	4000	0.35	0.24	0.11
IC 4651,Mel-169	340.08	-7.90	0.82	2400	0.25	0.11	0.14

= 2, while Liller 1 and UKS 1 have E(B-V)$\approx$ 3 (Table 2). The dust emission reddening can be much larger, in some cases exceeding E(B-V)$_{FIR}$ = 4 which occurs for Terzan 5, 10, 4, 1 and UKS 1. The lowest galactic latitude globular cluster Liller 1 has the highest value (E(B-V)$_{FIR}$ = 11.57).

For the old open clusters the largest reddening derived from the CMD occurs for Pişmiş 2 (E(B-V) = 1.48), and seven other clusters exceed E(B-V) = 1 (Table 3). Three clusters have dust emission reddening exceeding E(B-V)$_{FIR}$ = 5 which are IC 4291 (Pişmiş 18), Pişmiş 19 and finally NGC 6134 with E(B-V)$_{FIR}$ = 25.66. They are at extremely low latitudes and in directions not far from the galactic centre (Table 3) which can accumulate reddening from dust in several arms and the Molecular Ring (Sect. 2).
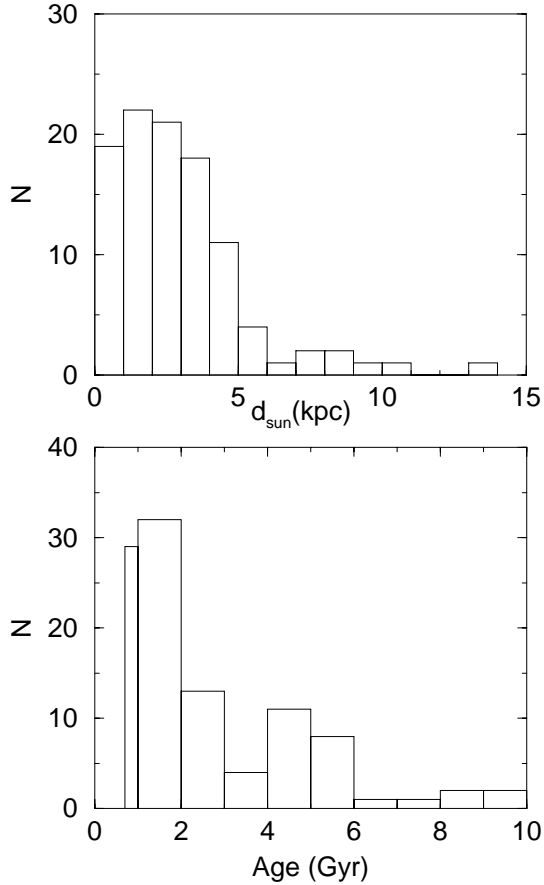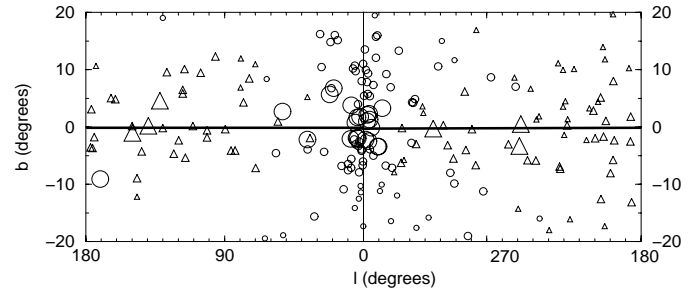
Fig. 4. Angular distribution in galactic coordinates for globular clusters (circles) and old open clusters (triangles) within $|b| < 20°$. The symbol size is proportional to reddening derived from the stellar content: (i) large corresponds to E(B-V)> 1.0; (ii) intermediate $0.2 \leq E(B-V) \leq 1.0$; and (iii) small E(B-V)< 0.2.

Fig. 3. Distance (upper panel) and age (lower panel) histograms for old open clusters. In the age histogram the first bin considers clusters in the range 0.7 to 1 Gyr.

4.1. $\beta E(B-V)$: possibility of background reddening

In order to check the possibility of background reddening in the directions of globular and old open clusters we define the difference $\beta E(B-V) = E(B-V)_{FIR} - E(B-V)$ (Tables 2 and 3, respectively). Fig. 6 shows $\beta E(B-V)$ histograms considering both samples together. For high latitude clusters ($|b| > 20°$) we find a tight gaussian distribution suggesting an error distribution. We

recall that E(B-V)$_{FIR}$ uncertainties typically amount to 16 % (Schlegel et al. 1998). The gaussian peak is in the bin 0-0.02, indicating a small offset between the two reddening types with higher values for E(B-V)$_{FIR}$. This can also be seen in Panel **a** of Fig. 5 as a small systematic shift of the points with respect to the identity function. There are two deviating objects in Panel **a** of Fig. 6 which are the globular cluster M 107 (NGC 6171) and the open cluster C 1901. For M 107 E(B-V)$_{FIR}$ = 0.45 and E(B-V) = 0.33 (Table 3), thus βE(B-V) = 0.12. Recently Salaris & Weiss (1997) derived E(B-V) = 0.38 from isochrone fitting on CCD photometry, and they remarked that, for this cluster, values in the literature are in the range $0.30 < E(B-V) < 0.48$. We suspect that the positions of M 107 in Figs. 5 and 6 reflect an uncertainty in the reddening derived from the stellar methods. On the other hand NGC 1901 with E(B-V)$_{FIR}$ = 0.33 and E(B-V) = 0.06 (Table 3) has the LMC disk as background (Sanduleak & Philip 1968), so that the high βE(B-V) = 0.27 must reflect dust emission from LMC complexes. Panels **b** and **c** deal with βE(B-V) histograms for low latitude clusters ($|b| < 20°$), respectively for $\beta E(B-V) < 1.5$ and high βE(B-V) values. Similarly to panel **a** there occurs in panel **b** a peak near zero (bin 0-0.04), which indicates that most points indeed closely follow the identity function (Panel **b** of Fig. 5). Thus, Schlegel et al.'s (1998) reddening values at low latitudes agree with those derived from stellar data for about two thirds of the clusters. Finally, the histogram for high βE(B-V) values (Panel **c**) shows 18 clusters with $\beta E(B-V) > 1.0$. These interesting objects together with the deviating clusters in Panel **b**, typically with $\beta E(B-V) > 0.30$, are discussed in detail in Sect. 4.4 for the possibility that their reddening values have an origin in the background dust.

Since mass loss is important in the last stages of red giant evolution dust accumulation in globular clusters is not unexpected. Cloudlets would contribute to differential reddening in CMDs as well as to 100 μm dust emission. Forte & Mendez (1988) found evidence for dust within globular clusters. They studied ten southern globular clusters, in particular NGC 362 and NGC 6624, and detected by means of CCD imaging regions with light deficiency which was attributed to dark clouds with intrinsic extinctions close to $A_V = 2.5$. Their sizes are on
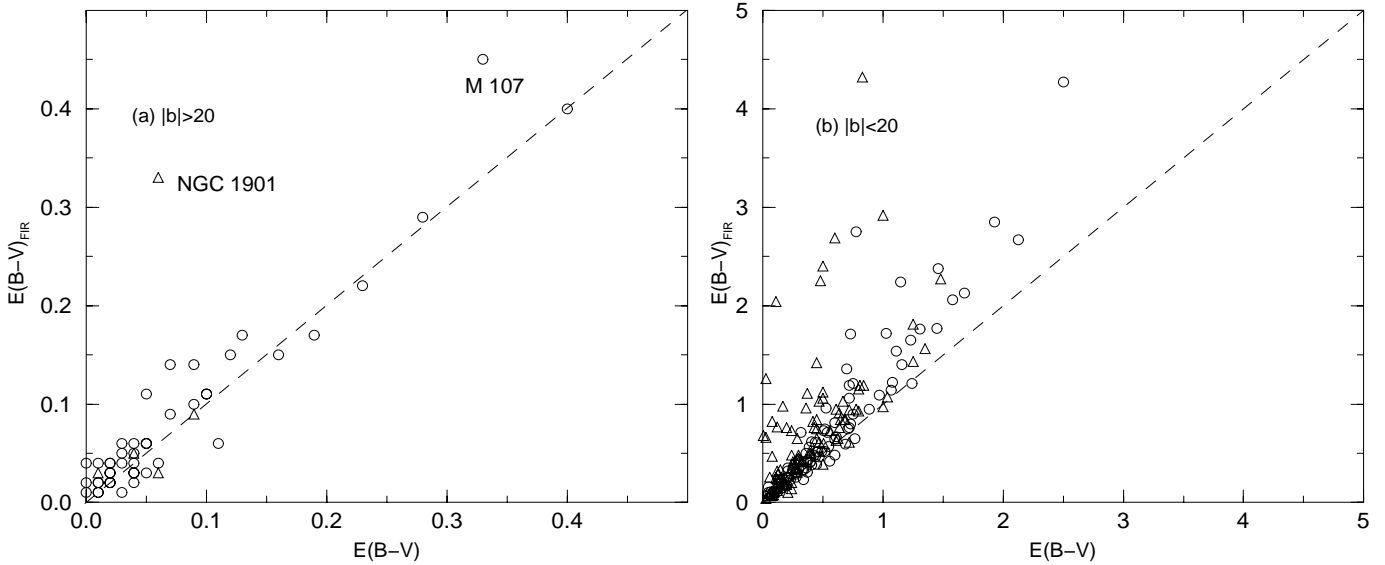
Fig. 5 shows E(B-V)$_{FIR}$ as a function of the reddening derived from the stellar content. Panel **a** contains the clusters with $|b| > 20°$, presenting a good agreement between the reddening values, except the clusters M 107 and NGC 1901 which are discussed in Sect. 4.1. The highest values at such latitudes are E(B-V)$_{FIR} \approx E(B-V) \approx 0.4$. Panel **b** contains the clusters with $|b| < 20°$ where most points follow the identity function up to E(B-V)≈ 1.0. However, an important fraction of points in the range $0 < E(B-V) < 1$ has large deviations in the sense of higher E(B-V)$_{FIR}$. For $E(B-V) > 1$ the points deviate systematically from the identity function in the sense that E(B-V)$_{FIR}$ values are higher. A possible interpretation would be dust contributions for E(B-V)$_{FIR}$ arising from the cluster background.

Fig. 5a and b. $E(B-V)_{FIR}$ versus $E(B-V)$ of the Galactic globular clusters (circles) and old open clusters (triangles). Panels: **a** high latitude objects ($|b| > 20°$), **b** low latitude ($|b| < 20°$). The dashed line represents the identity function. Note that in panel **b** a few very reddened objects ($E(B-V)_{FIR} > 5$) are beyond the figure limits (Tables 2 and 3).
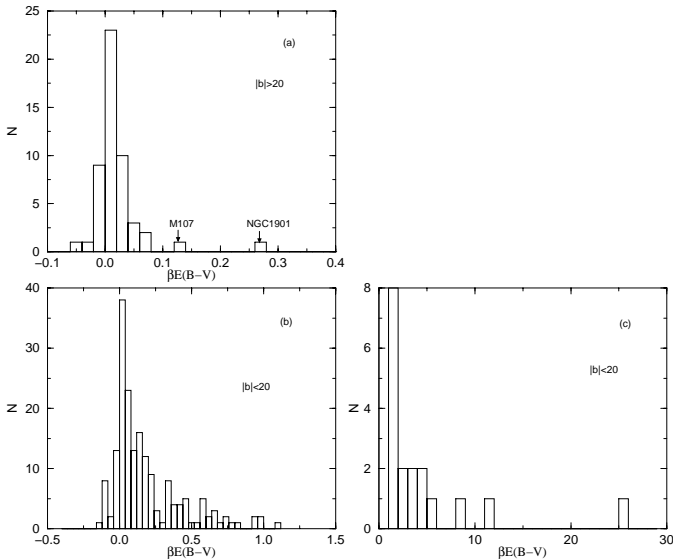

Fig. 6a–c. Histograms of $\beta E(B-V)$ for the total sample of globular clusters and old open clusters: **a** high latitude clusters, **b** low latitude clusters for $\beta E(B - V) < 1.5$ and finally **c** low latitude clusters for the entire $\beta E(B-V)$ range. The first bin in panel **c** is cropped for clarity purposes.

the order of tenths of a parsec and they occur near the cluster nucleus. We checked whether Schlegel et al.'s reddening values are sensitive to internal dust contributions in the clusters NGC 362 and NGC 6624. We extracted $E(B-V)_{FIR}$ values for a cross with 17 pixels in Schlegel et al.'s maps (each pixel has $2.4' \times 2.4'$). This cross samples the cluster main body and zones outside it, but still within the tidal radius (Trager et al. 1995). We noted fluctuations in $E(B-V)_{FIR}$ not exceeding 0.01 and 0.02, respectively. We conclude that Schlegel et al.'s reddening values

are not particularly sensitive to the cloudlets owing to the large pixel size and the cloudlets' small covering factor.

Star clusters within the dust layer as defined in Sect. 2.2 ($|Z'| \approx 200$ pc) are expected to have significant differences between $E(B-V)_{FIR}$ and $E(B-V)$ values. In order to study the behaviour of $\beta E(B-V)$ we considered the cluster perpendicular distance to the Galactic plane (Z') calculated with Eq. (1), using the data in Tables 2 and 3 for the globular and old open clusters. Fig. 7 shows $\beta E(B-V)$ as a function of Z' for four Z' ranges. Panel **a** shows objects up to 2 kpc from the Plane. Clearly, there is a large scatter of $\beta E(B-V)$ values within the 200 pc dust layer, together with a significant wing which extends to ≈ 400 pc. The scatter suggests that most of the differences between reddening values derived from dust emission and the stellar content are due to dust clouds in the disk background of the clusters. Panels **b**, **c** and **d** show the behaviour of $\beta E(B-V)$ in the regions increasingly away from the disk. In all three panels $\beta E(B-V)$ values are small which is consistent with the fact that all these objects are halo globular clusters. The only strongly deviating object in Panel **b** is NGC6144 (Sect. 4.4). In **b** and **c** the average $\beta E(B-V)$ value is slightly positive corresponding to the small offset caused by higher $E(B-V)_{FIR}$ values. Unless an extremely thin diffuse distribution occurs throughout the halo caused by e.g. cooling flows and/or debris from dwarf galaxies accreted by the Milky Way, this offset observed for halo globular clusters implies that either Schlegel et al.'s zero point is slightly overestimated or that intrinsic reference colors, spectral distributions and isochrones were exceedingly red. Finally, in Panel **d** the offset is not present, but the sample is small.

Large differences $\beta E(B-V)$ could be caused by the existence of dust clouds behind the clusters, primarily within the dust layer. In order to investigate this possibility we calculated cluster positions in the Galaxy and compared them to the assumed dust
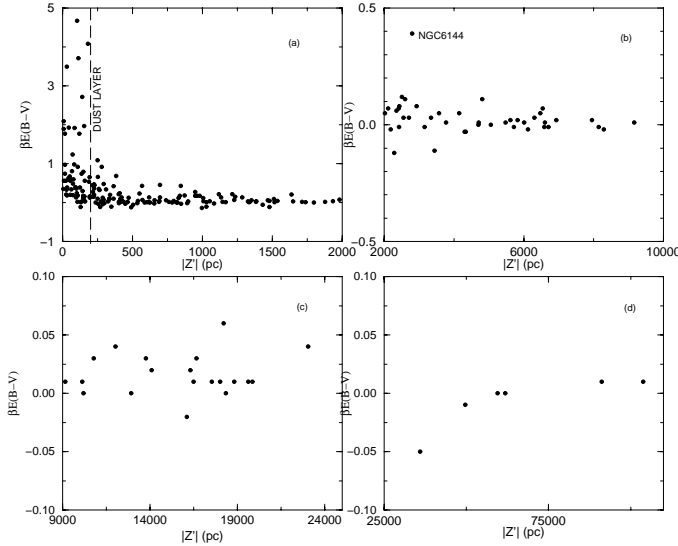
Fig. 7a–d. βE(B-V) for globular and old open clusters as function of distance from the Plane $|Z'|$ in parsecs. The four panels show distinct ranges of distances from the galactic plane. Note that the βE(B-V) scale becomes amplified from **a** to **d**. In panel **a** the dust layer of 200 pc is indicated and the values are cropped at βE(B-V) = 5.0.

layer distribution. The latitude with respect to the true Galactic plane is given by

$$\tan b' = \frac{Z'}{d \sin b} \tan b. \qquad (2)$$

Using this corrected latitude b' it is possible to calculate the perpendicular distance of the cluster to the true Galactic plane d', the distance along the cluster line of sight from the true Plane up to the dust layer edge d_{layer}, and for the clusters within the dust layer the path behind them d_{bck}:

$$d' = \frac{Z'}{\sin b'}, \ d_{\text{layer}} = \frac{200\,pc}{\sin b'}, \ d_{\text{bck}} = d_{\text{layer}} - d' \qquad (3)$$

where 200 pc refers to the conservative dust layer height, assumption of Sect. 2.2. We also assumed a galactic disk radius $R = 15$ kpc.

Fig. 8 shows in panel **a** and in the blowup **b** E(B-V)$_{\text{FIR}}$ as function of d_{layer}. We note in panel **a** that objects with large E(B-V)$_{\text{FIR}}$ values (e.g. NGC 6134, Pişmiş 19, Liller 1, IC 4291) have a large path length within the layer. This is expected since the reddening derived from dust emission (E(B-V)$_{\text{FIR}}$) should integrate dust contributions along the whole path throughout to the disk edge (d_{layer}). Panel **b** suggests two correlations with different slopes, which might indicate differences in the cumulative effect of dust emission due to a discrete distribution of dust clouds. In panels **c** and its blowup **d** the behaviour of βE(B-V) is shown as a function of the path behind the cluster up to the disk edge (d_{bck}). Panel **c** suggests that large βE(B-V) values for clusters like NGC 6134, Pişmiş 19, Liller 1, IC 4291 could arise from a dust cloud distribution behind the clusters since their directions and positions in the Galaxy imply a large background path up to the disk edge. Panel **d** shows considerable scatter

which might be due to different origins: (i) inhomogeneous distribution of dust clouds, (ii) considerable uncertainties, (iii) the assumptions of a dusty disk are not satisfactory. Notice that for the assumed dust layer height of 200 pc the clusters outside the dust layer ($d_{\text{bck}} = 0$) have a considerable range of values $0 < \beta E(B-V) < 1$. This suggests that the Milky Way dust lane could be thicker (Sect. 4.4).

4.2. Directions of some reddened young open clusters

Since the young disk is considerably thinner than the old disk (Janes & Phelps 1994; Friel 1995) it is worthwhile to study some interesting cases. We discuss some of the most reddened optical open clusters.

NGC 3603 and Westerlund 2 are clusters embedded in H II region complexes, where internal reddening is important. NGC 3603 ($\ell = 291.61°$, $b = -0.52°$) is located at a distance $d_{\text{sun}} = 7$ kpc and has E(B-V) = 1.44 from the CMD (Melnick et al. 1989), which comprises both the internal and foreground reddening. From the integrated spectrum Santos & Bica (1993) obtained a foreground reddening of E(B-V)$_f$ = 1.18, implying an internal reddening E(B-V)$_i$ = 0.26, by using a template spectrum which included internal absorption. Westerlund 2 ($\ell = 284.27°$, $b = -0.33°$) at a distance $d_{\text{sun}} = 5.7$ kpc has E(B-V) = 1.67 from the CMD (Moffat et al. 1991). Piatti et al. (1998b) derived E(B-V)$_f$ = 1.40 and E(B-V)$_i$ = 0.27 by means of an integrated spectrum analysis.

Westerlund 1 ($\ell = 339.55°$, $b = -0.40°$) is possibly the most reddened open cluster which can be optically observed. By means of CMDs and integrated spectrum Piatti et al. (1998b) derived E(B-V) = 4.3 and $d_{\text{sun}} = 1.0$ kpc.

From Schlegel et al.'s (1998) reddening map we obtained very high reddening values derived for these young disk objects at very low galactic latitudes: E(B-V)$_{\text{FIR}}$ = 59.7, 65.7 and 12.3 respectively for NGC 3603, Westerlund 2 and Westerlund 1. The extremely high E(B-V)$_{\text{FIR}}$ for NGC 3603 and Westerlund 2 are probably related to lines of sight intercepting dust cloud cores (Sect. 2), presumably the molecular clouds from which they were formed. Since Westerlund 1 is projected close to the Plane not far from the galactic center direction, its high E(B-V)$_{\text{FIR}}$ can be explained by the dust cumulative effect produced by a series of spiral arms and the Molecular Ring in that direction (Sect. 2.1).

4.3. Reddening in the Sagittarius dwarf direction

The globular clusters associated with the Sagittarius Dwarf are indicated in Table 1. Their E(B-V) values derived from the stellar content are comparable to those derived from the dust emission. Only a small systematic difference occurs, in the sense that values derived from dust emission are larger by βE(B-V) = 0.01-0.02. Assuming that M 54, Terzan 8, Arp 2 and Terzan 7 are slightly foreground or within Sagittarius itself, this sets a very low upper limit to the dust content in Sagittarius, in agreement with the fact that it is very depleted in H I (Koribalski et al. 1994).
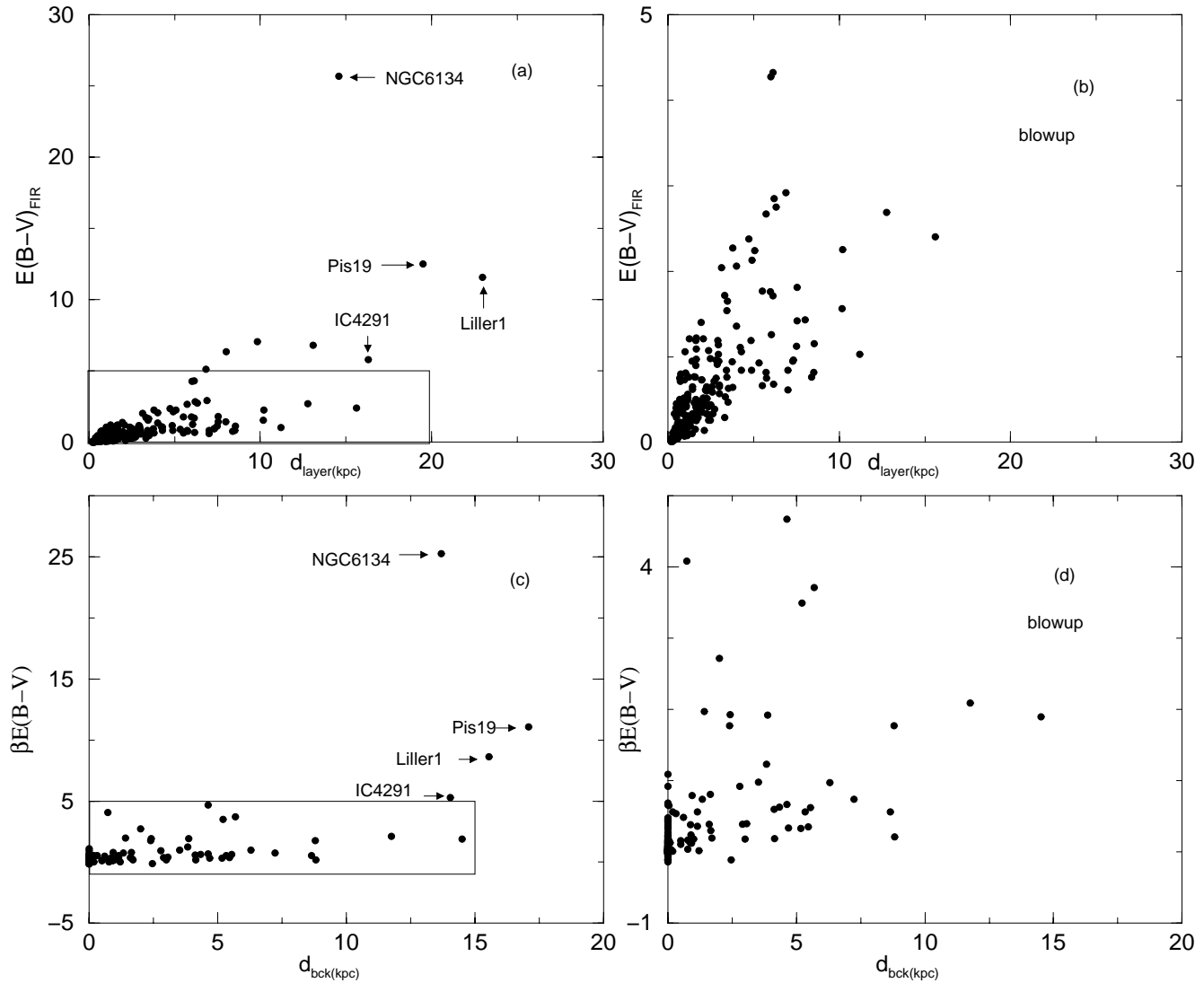
Fig. 8a–d. Panels: **a** Dust emission reddening E(B-V)$_{FIR}$ as a function of the distance in the cluster line of sight from the true Plane up to the dust layer edge d$_{layer}$, assuming a dust layer height of $|Z'| = 200$ pc; **b** blowup of **a**; **c** βE(B-V) as a function of background path between the cluster and the disk edge in that direction (d$_{bck}$); **d** blowup of **c**.

4.4. Evidence for dark clouds with $|Z'| > 200$ pc

Assuming the Milky Way dust layer height to be $|Z'| = 200$ pc, Table 4 presents the 60 clusters with βE(B − V) > 0.30, showing their height from the Plane $|Z'|$, the distance in the cluster line of sight from the true Plane up to the dust layer edge d$_{layer}$, and the path length behind the cluster up to the disk border d$_{bck}$. They are separated in two groups, one formed by clusters within the dust layer (10 globular and 33 old open clusters) and the other by clusters outside it (15 globular and 2 old open clusters). As discussed in Sect. 4.1 the large βE(B-V) values for clusters within the dust layer can be explained by dust clouds behind the clusters. The clusters outside the dust layer with large βE(B-V) values (see also their distribution in Fig. 7 and he wing in the distribution above the dust layer) might be explained by higher $|Z'|$ dust clouds. A well-known example is the high latitude dust cloud Draco Nebula at a height from

the Plane 300 to 400 pc (Gladders et al. 1998). In addition, star forming complexes as traced by means of Wolf-Rayet stars indicate that they are concentrated within a height from the Plane of 225 pc, but some attain 300 pc (Conti & Vacca 1990).

Assuming a dust layer height $|Z'| = 300$ pc there would remain only 7 clusters outside the dust layer (Table 4). This corresponds to 3% of the total sample of 250 star clusters in the present study. They are all globular clusters: Lyngå 7, NGC 6144, NGC 6256, NGC 6355, NGC 6380, Tonantzintla 2 and NGC 6401. Among these clusters only NGC 6144 is very far from the plane at $|Z'| \approx 2.8$ kpc (Table 4). Although NGC 6144 has no CCD photometry yet, the photographic CMD and the integrated light reddening estimates (Harris 1996 and references therein) are consistent at about E(B-V) ≈ 0.32. We suspect that E(B-V)$_{FIR} = 0.71$ for this cluster is overestimated, arising from foreground dust heated above the upper limit 21 °K (Schlegel et al. 1998) by the hot star σ Scorpii. Indeed, NGC 6144 is seen

Table 4. Distance from the plane and lines of sight for clusters with $\beta E(B-V) > 0.30$.

Clusters within dust layer

NAME	$|Z'|$ (pc)	d_{layer} (kpc)	d_{bck} (kpc)
Terzan 4	182	8.0	0.7
Liller 1*	6	22.9	15.5
Terzan 1	106	9.8	4.6
Terzan 5	120	6.0	2.4
Terzan 6	188	5.7	0.3
UKS 1	113	13.1	5.7
Terzan 9	155	6.3	1.4
Terzan 10	141	6.8	2.0
NGC 6544	85	6.1	3.5
Terzan 12	109	6.2	2.8
Be 81	87	6.9	3.9
IC 4756	55	1.6	1.2
NGC 6802	30	6.1	5.2
NGC 6866	193	1.5	0.1
IC 1369*	8	12.8	11.8
NGC 7226*	11	11.2	8.6
Ki19*	18	10.2	8.8
NGC 7762	93	1.6	0.9
Cr 463	73	1.0	0.6
IC 166*	5	8.5	5.5
Ki 7*	24	7.5	5.3
NGC 1496*	18	7.5	6.3
NGC 2194	93	5.7	3.1
Tr 5*	63	7.3	4.7
NGC 2236*	79	7.3	4.1
NGC 2112	159	1.0	0.2
Cr 110	52	7.5	5.5
NGC 2286	72	6.0	3.8
Haf 8	43	5.5	4.3
Haf 6*	28	8.4	5.2
NGC 2360*	17	8.5	7.2
NGC 2527	35	3.5	2.9
NGC 2533	50	6.2	4.6
NGC 2477	99	2.3	1.1
Piş 2	150	3.8	0.9
NGC 2660	136	4.2	1.3
NGC 3496*	7	15.6	14.5
IC 4291	27	16.3	14.0
Piş 19*	2	19.5	17.1
NGC 5823	45	3.1	2.4
NGC 5822	67	2.5	1.6
NGC 6005	125	4.3	1.6
NGC 6134	12	14.6	13.7

Notes to Table 4: * lines of sight are truncated considering a galactic disk radius R = 15 kpc.

Table 4. (continued)

Clusters outside dust layer

NAME	$|Z'|$ (pc)	d_{layer} (kpc)	d_{bck} (kpc)
Lyngå 7	311	4.3	0.0
NGC 6144	2801	0.7	0.0
NGC 6256	384	3.3	0.0
NGC 6355	696	2.1	0.0
Terzan 2	280	4.7	0.0
HP 1	252	5.1	0.0
NGC 6380	569	3.4	0.0
Tonantzintla 2	367	3.5	0.0
NGC 6401	847	2.8	0.0
Palomar 6	214	6.0	0.0
Djorgovski 1	227	4.9	0.0
ESO456-SC38	226	4.9	0.0
NGC 6553	254	4.0	0.0
NGC 6749	265	5.5	0.0
Palomar 10	295	4.0	0.0
Be 54	259	2.9	0.0
NGC 7044	226	3.0	0.0

ing star σ Scorpii is double (B2 III + O9.5 V), and ionizes the H II region Sh 2-9 (Sharpless 1959), or Gum 65 (Gum 1955). This hot double star also has its reflection nebula component Cederblad 130 (vdB-RN 104), which almost overlaps with the Antares reflection nebula. It is possible that dust grains in the direction of NGC 6144 are being heated by this particular configuration. At any rate CCD photometry of NGC 6144 is necessary to definitely establish the reddening E(B-V) affecting the cluster stars.

Howk & Savage (1999) detected high-Z dust structures in a sample of 7 edge-on spiral galaxies (NGC 891, NGC 3628, NGC 4013, NGC 4217, NGC 4302, NGC 4565 and NGC 4634). The thickness of the dust lanes in these galaxies is in the range $500 < 2 \times |Z| < 900$ pc. The high-Z dust features have typical dimensions of hundreds of parsecs and are located at heights in the range 500-1450 pc. The present study indicates the need of a Milky Way dust layer of thickness $2 \times |Z| \approx 600$ pc in order to explain the lines of sight of 97 % of the known intermediate age and old clusters. The remaining 3 % would require some higher Z clouds.

5. Concluding remarks

Since the 100 μm dust emission reddening maps of Schlegel et al. (1998) provide whole-sky reddening estimates with relatively high angular resolution it is important to explore them in detail for a better understanding of the dust properties in different directions.

We provided an overview of the distribution along the galactic plane and in some interesting latitude directions. The accumulation of dust clouds in different arms and large structures such as the Molecular Ring can be distinguished. Individual dust complexes, including their cores, have E(B-V)$_{FIR}$ values

through the edge of the ρ Ophiuchi dark cloud complex in the association Upper Scorpius at distance d_{sun} = 125 pc (de Zeeuw et al. 1999). The cluster pathsight crosses the reflection nebula illuminated by the red supergiant Antares, also designated as IC 4606, Cederblad 132 or vdB-RN 107 in the catalogue of reflection nebulae by van den Bergh (1966). The neighbour-

compatible with those of embedded clusters derived from infrared photometry. An exception is the Nuclear Region where the temperature in the Central Molecular Zone appears to be underestimated in the Schlegel et al.'s temperature maps.

The 100 μm dust emission reddening maps provide E(B-V)$_{FIR}$ values compatible to E(B-V) derived from the stellar content of globular and old open cluster for $\approx$ 75 % of the 250 directions probed in the present study ($\beta E(B-V) < 0.30$). The values for most high-latitude clusters ($|b| > 20°$) are in good agreement; these are objects in general outside the disk dust layer, so that all dust in the line of sight is sensitive to both methods. An interesting exception is NG C 1901 which is outside the dust layer and has a E(B-V)$_{FIR}$ much larger than E(B-V). The background dust source in this case is the LMC disk.

The differences between the dust emission and stellar content reddening values occur most frequently for low latitude clusters ($|b| < 20°$). Brightness selection effects due to reddening and distance particularly affect the open cluster sample. In the existing catalogues many intermediate age open clusters are yet to be studied, while future infrared surveys should reveal many new open clusters. These distant objects are expected to have increasing reddening values, but the $\beta E(B-V)$ values should decrease since the line of sight behind the cluster within the dust layer decreases. Most of the known globular clusters have CMDs, but infrared surveys should reveal some new ones in disk and bulge zones. Those far in the disk should behave like the heavily reddened far open clusters.

Bandwidth effects on the intrinsic reddening law have implications on the results for larger extinctions. The fact that most of the points follow a 1:1 FIR/Optical relation up to E(B-V) = 1.0 (Fig. 5) suggests that this effect should become important for reddening values beyond this limit. An additional complication for objects so heavily reddened that the stellar content can be studied only in the infrared is that the transformations to optical reddening values depend on grain properties.

From the spatial distribution of available objects and their relative positions with respect to the dust layer we conclude that background dust clouds are probably responsible for these differences. A dust layer with thickness $2 \times |Z| \approx 600$ pc is required to explain the distribution of $\approx$ 97 % of the sample. Some additional higher Z dust clouds, like the Draco Nebula, would also be required to explain the rest.

The present study of reddening in star cluster directions suggests that the Milky Way is similar in dust layer thickness and occurrence of some high-Z dust structures to edge-on spirals studied by Howk & Savage (1999). In particular the Milky Way dust layer may be thicker than previously thought.

References

Bania T.M., 1980, ApJ 242, 95
Barbuy B., Bica E., Ortolani S., 1998a, A&A 333, 117
Barbuy B., Bica E., Ortolani S., 1998b, A&AS 132, 333
Barbuy B., Ortolani S., Bica E., Desidera S., 1999, A&A 348, 783
Bica E., Ortolani S., Barbuy B., 1995, A&AS 120, 153
Bica E., Ortolani S., Barbuy B., 1999, A&AS 136, 363
Bica E., Clariá J.J., Piatti A.E., Bonatto C., 1998, A&AS 131, 483
Burstein D., Heiles C., 1978, ApJ 225, 40
Burstein D., Heiles C., 1982, AJ 87, 1165
Carpenter J.M., Meyer M.R., Dougados C., Strom S.E., Hillenbrand L.A., 1997, AJ 114, 198
Carraro G., Ng Y.K., Portinari L., 1998, MNRAS 296, 1045
Carraro G., Vallenari A., Girardi L., Richichi A., 1999, A&A 343, 825
Catchpole R.M., Whitelock P.A., Glass I.S., 1990, MNRAS 247, 479
Cohen M., 1995, ApJ 444, 874
Cohen R.S., Cong H., Dame T.M., Thaddeus P., 1980, ApJ 239, L53
Combes F., 1991, ARA&A 29,, 195
Comerón F., Rieke G.H., Burrows A., Rieke M.J., 1993, ApJ 416, 185
Comerón F., Rieke G.H., Rieke M.J., 1996, ApJ 473, 294
Conti P.S., Vacca W.D., 1990, AJ 100, 431
Da Costa G.S., Armandroff T.E., 1995, AJ 109, 25
de Zeeuw P.T., Hoogerwerf R., de Bruijne J.H.J., Brown A.G.A., Blaauw A.,, 1999, AJ 117, 354
Digel S., Bally J., Thaddeus P., 1990, ApJ 357, 29
Forte J.C., Mendez M., 1988, AJ 95, 500
Friel E.D., 1995, ARA&A 33, 381
Georgelin Y.P., Georgelin Y.M., 1970a, A&A 7, 133
Georgelin Y.P., Georgelin Y.M., 1970b, A&A 6, 349
Gladders M.D., Clarke T.E., Burns C.R., et al., 1998, ApJ 507, L161
Glass I.S., Moneti A., Moorwood A.F.M., 1990, MNRAS 242, 55
Gomez M., Lada C.J., 1998, AJ 115, 1524
Grabelsky D.A., Cohen R.S., Bronfman L., Thaddeus P., 1988, ApJ 331, 181
Gum C.S., 1955, Mem. R. Astron. Soc. 67, 155
Hammersley P.L., Garzón F., Mahoney T., Calbet X., 1995, MNRAS 273, 206
Harris W.E., 1996, AJ 112, 1487
Henderson A.P., 1977, A&A 58, 189
Howk J.C., Savage B.D., 1999, AJ 117, 2077
Hudson M.J., 1999, PASP 111, 57
Ibata R.A., Gilmore G., Irwin M.J., 1994, Nat 370,, 194
Janes K.A., Phelps R.L., 1994, AJ 108, 1773
Jones T.J., Mergeu J., Odewahn S., et al., 1994, AJ 107, 2120
Johnson J.J., Gehrz R.D., Jones T.J., Hackwell J.A., Grasdalen G.L., 1990, AJ 100, 518
Kaisler D., Harris W.E., McLaughlin D.E., 1997, PASP 109, 920
Kassis M., Janes K.A., Friel E.D., Phelps R.L., 1997, AJ 113, 1723
Kaluzny J., 1998, A&AS 133, 25
Kerr F.J., Hindman J.V., 1970, Aust. J. Phys. Ap. S. 18, 1
Krabbe A., Genzel R., Drapatz S., Rotaciuc V.,, 1991, ApJ 382, L19
Koribalski B., Johnston S., Optrupceek R., 1994, MNRAS 270, L43
Lada E.A., DePoy D.L., Evans II N.J., Gatley I., 1991, ApJ 371, 171
Lawson W.A., Feigelson E.D., Huenemoerder D.P., 1996, MNRAS 280, 1071
McGregor P.J., Harrison T.E., Hough J.H., Bailey J.A., 1994, MNRAS 267, 755
Melnick J., Tapia M., Terlevich R., 1989, A&A 213, 89
Mermilliod J.C., 1996, In: The origins evolution, and destinies of binary stars in clusters. ASP Conf. Ser. 90, p. 475
Minchin N.R., Hough J.H., McCall A., et al., 1991, MNRAS 248, 715
Moffat A.F.J., Shara M.M., Potter M., 1991, AJ 102, 642
Morris M., Serabyn E., 1996, ARA&A 34, 645
Nagata T., Woodward C.E., Shure M., Kobayashi N., 1995, AJ 109, 1676

Ortolani S., Bica E., Barbuy B., 1993, A&A 273, 415

Ortolani S., Bica E., Barbuy B., 1995a, MNRAS 284, 692

Ortolani S., Bica E., Barbuy B., 1995b, A&A 300, 726

Ortolani S., Bica E., Barbuy B., 1998, A&AS 127, 471

Ortolani S., Barbuy B., Bica E., et al., 1999a, A&A 350, 840

Ortolani S., Bica E., Barbuy B., 1999b, A&AS 138, 267

Ortolani S., Barbuy B., Bica E., 1999c, A&AS 136, 237

Piatti A.E., Clariá J.J., Bica E., Geisler D., Minniti D., 1998a, AJ 116, 801

Piatti A.E., Clariá J.J., Bica E., 1998b, A&AS 127, 423

Reipurth B., Rodríguez L.F., Chini R., 1999, AJ 118, 983

Rosino L., Ortolani S., Barbuy B., Bica E., 1997, MNRAS 289, 745

Salaris M., Weiss A., 1997, A&A 327, 107

Sanduleak N., Philip A.G.D., 1968, AJ 73, 566

Santos J.F.C. Jr., Bica E., 1993, MNRAS 260, 915

Schlegel D.J., Finkbeiner D.P., Davis M., 1998, ApJ 500, 525

Sharpless S., 1959, ApJS 4, 257

Strom K.M., Strom S.E., Merrill K.M., 1993, ApJ 412, 233

Trager S.C., King I.R., Djorgovski S., 1995, AJ 109, 218

van den Bergh S., 1966, AJ 71, 991

Webbink R.F., 1985, In: Goodman J., Hut P. (eds.) Dynamics of Star Clusters. Reidel, Dordrecht, p. 541